A two-scale finite element model for the fatigue design of large welded structures

H. Heyraud [a,b,*], C. Robert [a], C. Mareau [a], D. Bellett [a], F. Morel [a], N. Belhomme [b], O. Dore [b]

[a] Arts et Metiers Institute of Technology, LAMPA, HESAM Université, F-49035 Angers, France
[b] Manitou Group, Rue de l'Aubiniere, B.P. 249, 44150 Ancenis, France

Keywords:
Welded joints
Finite element analysis
High cycle fatigue
Multiaxial fatigue
Stress singularity

A B S T R A C T

Weld toes and weld roots of continuously welded structures subjected to cyclic loading are critical zones in terms of the fatigue resistance. The finite element method coupled with a fatigue criterion is commonly used to ensure the correct sizing and fatigue design of welded structures. However, weld geometries are often simplified or idealized to limit computational cost. In this work, a numerical two-scale approach is proposed in order to calculate a non-local multiaxial equivalent stress at the weld toe and the weld root from a global finite element shell model.

The influence of the parameters of the proposed model on the stiffness behaviour is investigated for three welded structures and for different loading cases. A comparison in terms of stiffness with other models from the literature is also proposed. The results show that the stiffness behaviour is not affected by the parameters of the proposed approach and that it is the most robust model for the different geometries and loading cases studied. The variation in the non-local multiaxial equivalent stress as a function of the parameters of the proposed approach was also studied. The comparison with full solid finite element models makes it possible to define minimum values for the different parameters studied and validates the potential of the proposed approach for the fatigue design of welded structures.

1. Introduction

The welding process is widely used for the fabrication of lifting and material handling equipment. Indeed, this process makes it possible to manufacture complex-shaped structures at high production rates, at least when compared to other joining process such as riveting. The welded structures used for telehandler chassis (see Fig. 1) are commonly made of S355 structural steel sheets with thicknesses ranging from 8 to 40 mm. During their service lives, telehandlers are submitted to very complex loading paths, and even though the yield strength is not exceeded, the repeated stressing caused by service loadings may lead to fatigue failure. The role of weld toes and weld roots, which act as stress concentration and often crack initiation sites, must therefore be considered when designing structural parts against fatigue failure. This aspect is important for telehandler chassis, for which the total seam weld length usually exceeds 50 meters.

The high cycle fatigue resistance of welds can be assessed by either global or local approaches and by the use of Wöhler curves [1].

* Corresponding author at: Arts et Metiers Institute of Technology, LAMPA, HESAM Université, F-49035 Angers, France.
E-mail address: hugo.heyraud@ensam.eu (H. Heyraud).

https://doi.org/10.1016/j.engfailanal.2021.105280

- For the application of the global approach, the cross-sectional area is used to calculate the nominal stress. Each welded detail is assessed using a specific Wöhler curve. While the application of this approach is straightforward, it requires a specific Wöhler curve for each type of welding detail, hence an extensive experimental database is required.
- Local approaches consider the stress concentration at the root of the notch where the crack will initiate. Given the variability in the local geometry at these locations, the fatigue life is commonly estimated from the maximal principal stress at the notch assuming a root radius of 1 mm [2]. In contrast with the global approach, only a single Wöhler curve (FAT225) is required for the fatigue design of the weld toes and weld roots. However, the stress state in the stress concentration zones must be accurately evaluated for the application of the local approach. This approach is therefore expensive from a computational point of view, especially for large structures.
- The structural stress approach is a trade-off between global and local approaches. It includes stress raising effects of the welded area without considering local stress concentrations. The advantage of this approach is that it requires fewer Wöhler curves when compared to the global approach.

The aforementioned methods are well adapted to the design of geometrically simple welded structures but are difficult to implement in an industrial context. Indeed, because they require either extensive experimental datasets or important computational resources, these approaches are difficult to apply to large or complex welded structures.

To circumvent these limitations, alternative approaches have been developed. For instance, Fayard et al. [3] proposed meshing rules and kinematic equations to consider the stiffness of continuously welded thin sheet structures. The fatigue design is based on the Dang Van [4] multiaxial fatigue criterion calculated from the hot spot stress defined by Radenkovic [5]. This approach, which requires only one Wöhler curve, is well suited for the situation where cracks initiate from weld toes. Fermér and Svensson [6] proposed a similar approach to evaluate the fatigue life of thin sheet welded structures. However, instead of kinematic equations, the local stiffness of the weld is estimated with an inclined shell element and the fatigue design is based on the structural stress concept. For a given stress distribution within the plate thickness and using the equilibrium equations, the structural stress is expressed according to a membrane and bending component of the stress tensor. The proportion of the bending component makes it possible to select the correct Wöhler curve to use. To deal with crack initiation at the weld roots, Turlier et al. [7] extended the approach of Fermér and Svensson [6]. Specifically, the structural stress is calculated from nodal forces and nodal moments [8] in order to limit the mesh-size influence. The fatigue life at weld toes is estimated from the FAT90 and the FAT100 Wöhler curves [1] while the FAT80 Wöhler curve is used for weld roots [9]. Crack initiation in welded structures can also be assessed using the notch stress intensity factor as a fatigue crack initiation parameter [10,11], or by strain energy approaches [12,13].

The present work is the continuation of the work of Fayard et al. [3] and Turlier et al. [7]. The welded connections encountered in a chassis structure are geometrically complex. As a result, the global and structural approaches, which are based on shell elements and/or an idealization of the weld [3,6,7], are difficult to set-up in a systematic fashion. Turlier et al. [14] compared the stiffness of the Fayard [15] and Turlier et al. [7] approaches on different elementary welded configurations and for different loading conditions. For certain cases, the difference between both models exceeds 15% and show the limits of these approaches.

Also, except for the nominal and the structural stress approaches of the IIW [1], it is not possible, with the aforementioned approaches, to simultaneously consider the impact of the stress multiaxiality and stress gradients. However, as discussed by Radaj and Sonsino [16] and Zettlemoyer and Fisher [17], these two factors influence the fatigue resistance of welded structures. On the other hand, local approaches allow the evaluation of stress gradients in a multiaxial context but the computational cost is often prohibitive for large structures.

In the present work, a strategy to consider welding details using the finite element method for complex and large welded structures is proposed. The objectives of this method are twofold. Firstly, the method should be capable of correctly evaluating the stiffness of a weld detail, which is necessary to estimate the mechanical response of the structure. The second aim is to accurately compute the stress field around welds, which is essential for considering the stress multiaxiality and the stress gradients in the context of the high cycle fatigue. The proposed method, which is detailed in the first part of this paper, relies on a two-scale approach. This makes it possible to

Fig. 1. Telehandler Manitou MT1840 and a closer view of typical welded connections found on the chassis.

estimate the fatigue resistance of complex structures with limited computational cost. In the second part, a comparative study is carried out to validate the proposed method. Specifically, the stiffness and local stress fields are compared to reference results for different weld details.

2. Description of the proposed method

2.1. Two-scale approach

Two contradictory goals must be accomplished when designing a large welded structure against fatigue failure. On one hand, the computational cost must be reasonable so that different design solutions can be explored. The consequence is that, in the context of the finite element method, shell elements are often used to model large structures. On the other hand, for the estimation of the fatigue resistance, the stress state in critical zones (i.e. weld toes and weld roots) must be determined. As such, weld details need to be modelled with solid elements, especially when one wants to consider stress gradients and stress multiaxiality. The drawback is that the computational cost drastically increases when solid elements are introduced in a model. A possible strategy to deal with these contradictory goals is to use a sub-modelling technique. Generally speaking, as discussed by Dal Cero Coehlo [18], a global shell element model is first used to identify the critical zones. Then, local solid elements sub-models are used for the fatigue assessment in these critical zones. However, with such an approach, the boundary conditions used in the sub-models, which are obtained from the global model, may not be realistic.

In the present work, as shown in Fig. 2, the strategy used to overcome the aforementioned difficulties is to model the seam welds using a two scale approach. At the local scale, welded details are modelled with solid elements in order to evaluate the local stress field. At the global scale, the metal plates are modelled with shell elements to limit the computational cost. However, instead of directly inserting the weld details into the global model, which would be computationally expensive, an intermediate step is used. Specifically, the idea is to propose a strategy to connect shell elements to solid elements. Then, the equivalent stiffness is estimated independently for each weld detail with a local model using both solid and shell elements. The weld details are therefore represented only with their equivalent stiffness matrices for the estimation of the global response of the welded structure. With this strategy, none of the degrees of freedom associated with a weld detail is included in the global shell model. The nodal displacements obtained from the global shell finite element model are then introduced as boundary conditions for local models. The final post-processing step consists of using an appropriate fatigue criterion with the resulting stress field, to estimate the fatigue life.

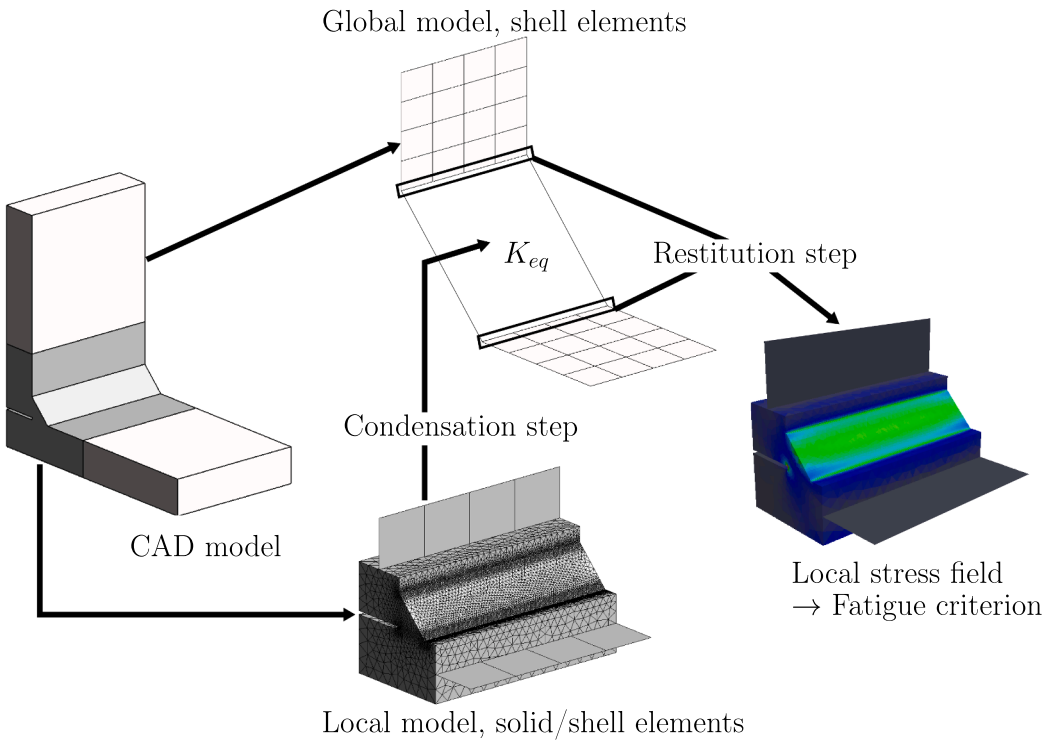

Fig. 2. Description of the two-scale approach used for the evaluation of the fatigue resistance of a welded structure.

2.2. Connection between solid and shell elements

As shown in Fig. 2, a local finite element model of a weld detail consists mostly of solid elements. Nevertheless, in order to insert it into the global model, some shell elements are used. As a result, in order to ensure the continuity of the displacement field at the interface between the solid elements and the shell elements, coupling equations must be used. If it is assumed that an isotropic linear elastic material model can be used, the connection can be defined by equating the work done on either side of the mixed dimensional interface [19,20] or by using shell element edge shape functions [21]. The second option has been chosen here. To establish the coupling equations, one must consider:

- the displacements at the solid element nodes;
- the displacement at the shell element nodes;
- the rotations at the shell element nodes;
- the shell element shape functions;

For the purpose of connecting solid and shell elements, the nodal displacement $\boldsymbol{U}(\mathrm{M})$ of a solid element node M at a solid/shell interface, such as the one shown in Fig. 3, is decomposed into two contributions:

$$\boldsymbol{U}(M) = \boldsymbol{U}^S(M) + \boldsymbol{U}^P(M) \tag{1}$$

The contribution $\boldsymbol{U}^S(\mathrm{M})$ is obtained from the direct interpolation of the nodal displacements of neighbouring shell elements while the contribution $\boldsymbol{U}^P(\mathrm{M})$ is due to the Poisson effect. The contribution $\boldsymbol{U}^S(\mathrm{M})$ is given by:

$$\boldsymbol{U}^S(M) = \sum_{k=1}^{2} (\mathbf{u}^{\mathbf{k}} + (\mathbf{v} \cdot \mathbf{e_z})\Phi \cdot \boldsymbol{\theta}^k) h_k(\eta) \tag{2}$$

In the above equation, $\boldsymbol{u}^k$ and $\boldsymbol{\theta}^k$ respectively correspond to the nodal displacement and nodal rotation vectors of the shell element node S_k at the interface. Also, $h(\eta) = (1 \pm \eta)/2$ is the first order shell element edge shape function when $\eta = \pm 1$. The unit vector $\mathbf{e_z}$ is the normal to the shell element plane and $\mathbf{v}$ corresponds to the vector $\mathbf{S_1M}$. The second order skew-symmetric tensor $\Phi$is built from the components of the $\mathbf{e_z}$ unit vector:

$$\Phi = \begin{bmatrix} 0 & e_{z_3} & -e_{z_2} \\ -e_{z_3} & 0 & e_{z_1} \\ e_{z_2} & -e_{z_1} & 0 \end{bmatrix} \tag{3}$$

Eq. (2) couples the six degrees of freedom of the shell element nodes to the three degrees of freedom of the solid element nodes at the solid/shell element interface. To include the Poisson effect along the direction normal to the shell element plane (i.e. direction $\mathbf{e_z}$), the associated component of the displacement field can be deduced from the out-of-plane strain components of shell elements. Specifically, under the assumption of a plane stress state, the components of the strain tensor are given by:

$$\epsilon_{11} = \frac{1}{E}\sigma_{11} - \frac{\nu}{E}\sigma_{22} \tag{4}$$

$$\epsilon_{22} = \frac{1}{E}\sigma_{22} - \frac{\nu}{E}\sigma_{11} \tag{5}$$

$$\epsilon_{33} = -\frac{\nu}{E}\sigma_{11} - \frac{\nu}{E}\sigma_{22} \tag{6}$$

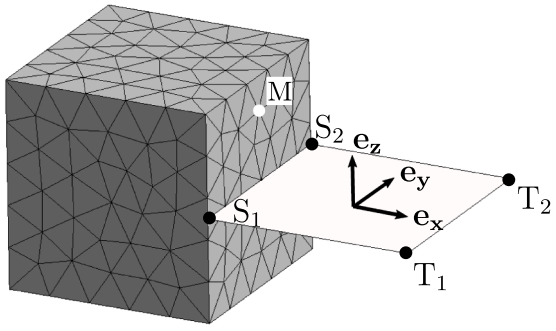

Fig. 3. Interface between shell elements and solid elements in a local finite element model. The three degrees of freedom of a solid element node (M) are connected to the six degrees of freedom of the corresponding shell element nodes (S_1, S_2, T_1, T_2).

$$\epsilon_{12} = \epsilon_{21} = \frac{1+\nu}{E}\sigma_{12} \tag{7}$$

$$\epsilon_{23} = \epsilon_{32} = 0 \tag{8}$$

$$\epsilon_{31} = \epsilon_{13} = 0 \tag{9}$$

where E is the Young's modulus and ν is the Poisson's ratio for the material of interest. The out-of-plane component of the strain tensor ϵ_{33} is then conveniently expressed from the in-plane components with:

$$\epsilon_{33} = \frac{-\nu}{(1-\nu)}(\epsilon_{11} + \epsilon_{22}). \tag{10}$$

To consider the Poisson effect in the constraint equations, the strain components $\epsilon_{\alpha\alpha}$ of Eq. (10) are expressed in terms of the nodal displacements of the shell element nodes. Specifically, the contribution $\boldsymbol{U}^P(M)$ is:

$$\boldsymbol{U}^P(M) = \sum_{k=1}^{2}(\mathbf{v}\cdot\mathbf{e_z})\left(\frac{-\nu}{(1-\nu)}\right)\left\{\left(\left[\frac{\mathbf{w^k}-\mathbf{u^k}}{D_1}\right]h_k\right)\cdot\mathbf{e_x} + \left(\frac{\mathbf{u^1}-\mathbf{u^2}}{D_2}\right)\cdot\mathbf{e_y}\right\}\mathbf{e_z} \tag{11}$$

where $\mathbf{w^k}$ is the nodal displacement vector associated with the shell element nodes T_k away from the interface. The distances D_1 and D_2 correspond respectively to the norm of the vectors $\mathbf{S_1T_1}$ and $\mathbf{S_2T_2}$. The unit vector $\mathbf{e_x}$ corresponds to the normal to the solid/shell interface and the vector $\mathbf{e_y}$ is such that $\mathbf{e_y} = \mathbf{e_z}\times\mathbf{e_x}$.

To account for the Poisson effect, the assumption of plane stress state has been made. However, close to a notch, the local stress field can be triaxial. Hence, a minimum distance between the weld toe and the solid/shell interface must be defined in order to limit its influence on numerical results. The local model uses two geometrical parameters, denoted by L_1 and L_2 and whose definition is illustrated in Fig. 4. The influence of the parameters L_1 and L_2 on the stiffness behavior and on the local stress state is discussed in Sections 3.1.1 and 3.2.1.

2.3. Equivalent stiffness matrix

To accurately estimate the stress field with the local model of a weld detail, a fine mesh must be used in the vicinity of the weld toes and the weld roots. As a result, the size of the stiffness matrix K_l associated with a local model, which connects the nodal displacements U to the nodal forces F, can be very large. As a consequence, local models cannot be directly inserted into the global model of a welded structure without requiring significant computational resources. To circumvent this issue, the proposed strategy is to evaluate the equivalent stiffness matrix K_e, whose size is much smaller than that of the original matrix K_l, for each local model. The stiffness matrix K_l associated with a local model can be written as:

$$[K_l] = \begin{bmatrix} K_{solid} & 0 & K_\lambda^t \\ 0 & K_{shell} & \\ K_\lambda & & 0 \end{bmatrix} \tag{12}$$

where K_{solid} is the stiffness matrix associated with the solid element part, and K_{shell} is the stiffness matrix associated with the shell element part of the local model. The constraint equations between the solid/shell element parts are included in the stiffness matrix K_l as Lagrange multipliers K_λ. For the purpose of calculating the equivalent stiffness matrix of a local model, a distinction is made between

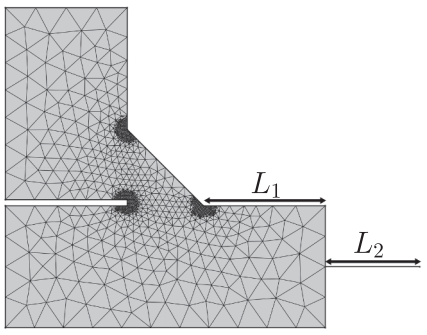

Fig. 4. Local model of a weld detail with solid and shell elements. The geometrical parameter L_1 is the length between the notch root and the solid/shell element interface. The geometrical parameter L_2 is the length of the connected shell element.

master nodes (U_m,F_m), which are common to the local and global models, and slave nodes (U_s,F_s), which exist in the local model only (see Fig. 5).

For the condensation of K_l into K_e, the following linear system is solved by imposing a unit displacement on one degree of freedom of the master nodes while the other degrees of freedom of the master nodes are set to zero:

$$\begin{bmatrix} K_{solid} & 0 & K_\lambda^t \\ 0 & K_{shell} & \\ K_\lambda & & 0 \end{bmatrix} \begin{Bmatrix} U_s \\ U_m \\ 0 \end{Bmatrix} = \begin{Bmatrix} F_s \\ F_m \\ \lambda \end{Bmatrix}. \tag{13}$$

The equivalent stiffness matrix K_e, which defines the relationship between the nodal displacements U_m and the nodal forces F_m at the master nodes, is constructed from the concatenation of the nodal force vectors at the master nodes resulting from the application of a unit displacement on one degree of freedom of a master node. Once the equivalent stiffness matrices have been computed for each weld detail, they are injected into the global model. The global model of the welded structure is thus composed of shell elements and the equivalent stiffness matrices corresponding to the different weld details (see Fig. 2). The solution to the global problem is then obtained from the finite element method.

For the purpose of evaluating the fatigue resistance of a weld detail, a restitution step is performed. This step consists of extracting the nodal displacements at the master nodes from the solution to the global problem. In the context of linear elasticity, the nodal displacement at the slave nodes for a welding detail are computed by superposing the solutions obtained for a unit nodal displacement on the corresponding master nodes. The strain field $\boldsymbol{\varepsilon}$ is then obtained from the nodal diplacements on both slave and master nodes. The stress field $\boldsymbol{\sigma}$ is finally computed from the strain field using a linear elastic isotropic constitutive model.

2.4. Non local multiaxial fatigue criterion

To account for the presence of stress gradients, the critical distance approach is used. This approach can take the form of either a point method, a line method or a volume method [22], see Fig. 6. Due to the type of structure studied here, as well as the numerous possible loading modes, the direction of the highest stress gradient can be difficult to identify. Hence, as the volume approach does not require this information, it is preferred here. The efficiency of this approach for notched components has been demonstrated by Taylor [23], Taylor [24] and Livieri and Tovo [25]. Also, to account for the influence of a multiaxial stress field, this approach can easily be coupled with a multiaxial criterion [26,27].

A local fatigue criterion can be defined as a function of (i) the stress state history and (ii) certain material parameters. If the loading cycle period is denoted by T, a local fatigue indicator σ_{eq} at position $\boldsymbol{x}$ can be calculated as follows:

$$\sigma_{eq}(\boldsymbol{x}) = E([\boldsymbol{\sigma}(\boldsymbol{x},t)]_T, a_{\alpha=1,n}) = 1 \tag{14}$$

where E is the fatigue function, $a_1 \ldots, a_n$ are n material parameters characterizing the fatigue resistance of the material. The material parameters are usually determined from the fatigue strengths obtained from different loading modes. It is worth mentioning that these parameters can depend on position $\boldsymbol{x}$ if material property gradients need to be considered.

In the context of a non-local approach, it is convenient to introduce a volume-averaged equivalent stress Σ_{eq} such that:

$$\Sigma_{eq}(\boldsymbol{x}) = \frac{1}{V(\boldsymbol{x})}\int_V \sigma_{eq}(\boldsymbol{x}')\ dv. \tag{15}$$

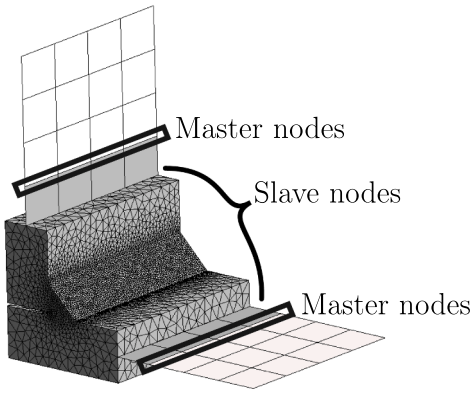

Fig. 5. Definition of master nodes and slave nodes for a local model. Master nodes are used to connect the local model to the global model. Slaves nodes are the remaining nodes of the local model.

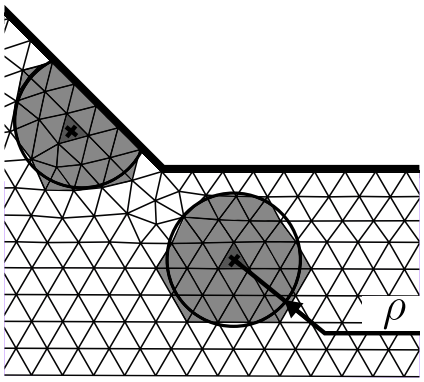

Fig. 6. 2D representation of the integration sphere. The parameter ρ defines the radius of the integration sphere for the computation of the non-local fatigue criterion.

As illustrated by Fig. 6, V is defined as a spherical volume, centred at each centroid of finite element, with radius ρ. The spatial position of the centroid of each finite element is used to identify the finite elements inside the integration sphere. The local fatigue indicator Σ_{eq} is then calculated from the volume averaged stress tensor of corresponding elements.

The above relation makes it possible to design welded structures against failure. It accounts for the effects of stress gradient and stress multiaxiality. According to the multiaxial fatigue criterion chosen, different parameters must be identified from different fatigue tests, other than the radius ρ of the integration volume V.

3. Validation

The strategy discussed in the previous section should make it possible (i) to consider the stiffness of a weld detail and (ii) to evaluate a non-local multiaxial fatigue criterion. To validate these aspects, the results obtained with the present strategy are compared to reference results presented in this section. The reference results used for the purpose of validation have been extracted from finite element simulations carried out with only 3D geometries using solid elements for different elementary welded structures. These structures are meshed with second-order tetrahedral elements. For the application of the proposed method, the solid part is meshed with second-order tetrahedral elements while the shell part is meshed with $Q4\gamma24$ elements [28]. The $Q4\gamma24$ element is a four nodes quadrilateral shell element with six degrees of freedom per node, including three translations and three rotations. This element is formulated from the combination of a plate element and a membrane element. In stress concentration zones, the element edge size is 0.08 mm for both model types. The size of the shell element in the proposed model is approximately 4 mm. An in-house finite element software, which is based on the finite-element mesh generator GMSH [29] and on the MUMPS solver [30], has been developed to apply

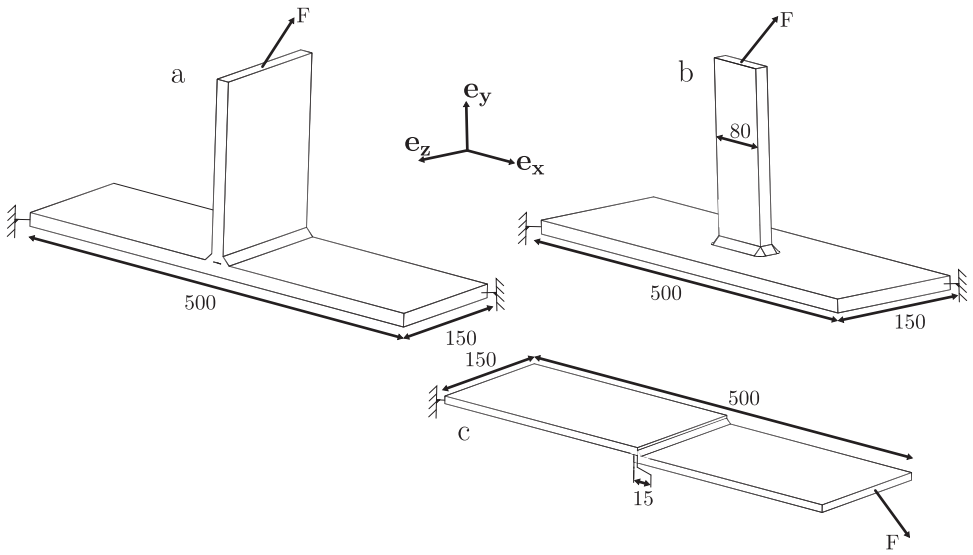

Fig. 7. Description of the three elementary welded structures used for validation: T-shaped joint (a), gusset (b) and lap joint (c). The boundary conditions are also indicated.

the proposed approach.

The elementary welded structures studied to validate the stiffness behaviour and the fatigue criterion are: a T-shaped joint, a gusset, and a lap joint. These structures are made with 15 mm thick steel plates, they have a weld throat thickness of 6 mm, and a gap at the weld root. The weld toes and the weld roots are modeled using a sharp angle, no fictitious notch rounding is considered. The geometries and the corresponding boundary conditions are shown in Fig. 7. For each elementary welded structure three loading cases are considered. These cases correspond to the application of a 1 kN force in either the $\boldsymbol{e}_x, \boldsymbol{e}_y$ or $\boldsymbol{e}_z$ directions.

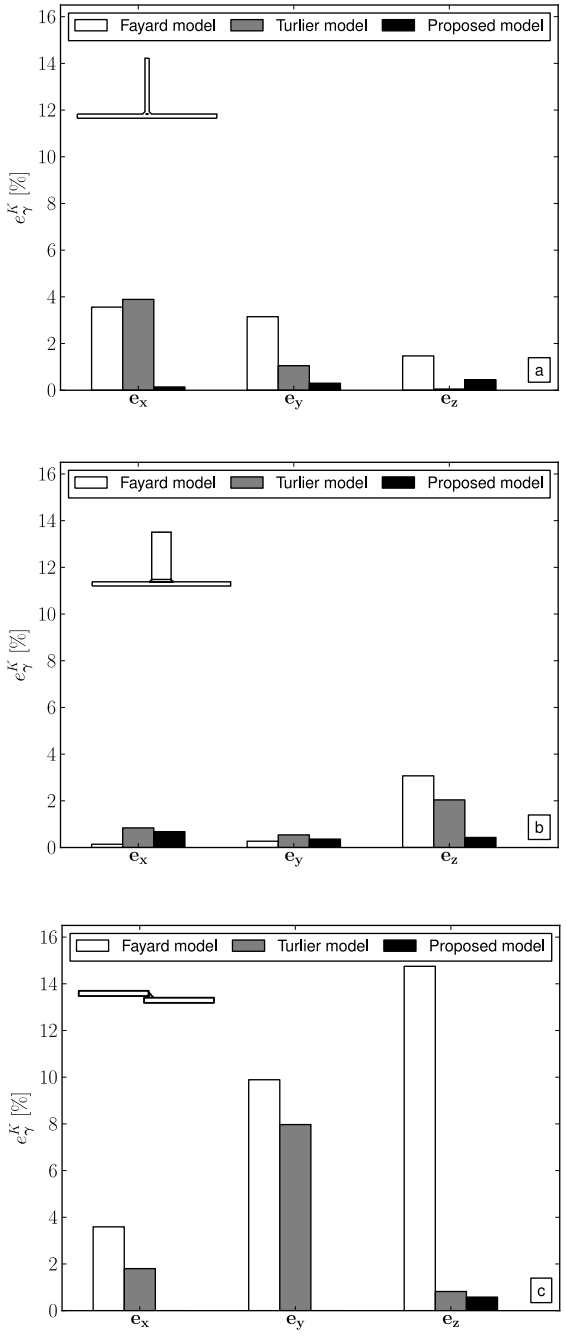

Fig. 8. Relative error indicator e_γ^K obtained when comparing the results of the proposed approach, the Fayard [15] approach and the Turlier et al. [7] approach to the reference results. Three different welded structures are considered: T- shaped joint (a), gusset (b) and lap joint (c). Three different loading directions are prescribed: $\boldsymbol{e}_x, \boldsymbol{e}_y$ an.d $\boldsymbol{e}_z$.

3.1. Global stiffness

To discuss the estimation of the stiffness with the proposed approach, the stiffness K_γ along the $\boldsymbol{\gamma}$ direction (where $\boldsymbol{\gamma} = \boldsymbol{e}_x, \boldsymbol{e}_y$ or $\boldsymbol{e}_z$) has been evaluated by computing the ratio between the applied load F_γ and the resulting displacement U_γ calculated at the boundary where the forces are applied (see Fig. 7). In order to compare the stiffness of different models, a relative error indicator e_γ^K is used:

$$e_\gamma^K = \frac{|K_\gamma^r - K_\gamma|}{K_\gamma^r} \tag{16}$$

where K_γ^r is the stiffness of the reference model while K_γ is that of the model being evaluated.

3.1.1. Influence of the L_1 and L_2 parameters

As discussed in Section 2.2, the proposed approach uses two geometrical parameters, denoted by L_1 and L_2, for the construction of the local model associated with a weld detail. To choose these parameters, their influence on the stiffness must be studied. For this purpose, the relative stiffness difference e_γ^K has been calculated for the different weld details for values of L_1 and L_2 ranging from 2 to 24 mm. The maximum stiffness difference is obtained for the T joint structure when loaded along the $\boldsymbol{e}_z$ direction. However, the stiffness difference is only 0.68%, which is negligible for most practical applications. This also indicates that the L_1 and L_2 parameters have little influence on the evaluation of the stiffness of a weld detail.

3.1.2. Comparison with some other models

To evaluate the stiffness of a weld detail, Fayard [15] and Turlier et al. [7] proposed approaches based on shell elements. For illustration purposes, the results obtained with the present approach are compared to those of Fayard [15] and Turlier et al. [7] as well as to the reference results for the different welded structures. The L_1 and L_2 have been fixed to 4 and 6 mm for the present approach. For the application of the Fayard [15] and Turlier et al. [7] approaches, the welded structures are meshed with first-order quadrilateral shell elements. RBE2 and RBE2-RBE3 elements are also used for the consideration of kinematic equations. For each welded structure, the total number of degrees of freedom used is similar for the different approaches. The NX NASTRAN software has been used for the application of the finite element method. The relative stiffness difference is plotted in Fig. 8 for the different configurations.

For most of the investigated situations, the proposed approach provides the most accurate estimation of the stiffness. There are a few situations for which the Fayard [15] and Turlier et al. [7] provide some better estimations, but the maximum relative error with respect to the stiffness is $e_{e_x}^K \approx 0.68\%$ (for the gusset structure loaded along the $\boldsymbol{e}_x$ direction, see Fig. 8b). The difference between the Fayard [15] approach and the reference model is up to $e_{e_z}^K \approx 14.8\%$ for the lap joint structure, and although the Turlier et al. [7] approach generally provides reasonable estimates of the stiffness, a maximum error of $e_{e_y}^K = 8.0\%$ is obtained for the lap joint structure. These results highlight the limits of the strategies used by Fayard [15] and Turlier et al. [7], which fail to provide accurate estimate of the global stiffness behaviour in certain situations, even though this aspect is critical for the correct evaluation of the stress field history in a welded structure.

3.2. Local stress state

To evaluate the ability of the proposed approach to correctly estimate the fatigue resistance, a non-local fatigue criterion is calculated. It is then compared to the reference results obtained from finite element simulations with only solid elements. In the following, the Dang Van [4] fatigue criterion is used. According to Fayard et al. [3] and Callens and Bignonnet [31], this criterion [4] can take into account the stress multiaxiality in welded structures. The criterion uses the maximum shear stress amplitude τ_a and the hydrostatic stress p. For a material point, this criterion takes the following form:

$$\sigma_{eq}(\boldsymbol{x}) = \max_{\mathbf{n}} \left(\max_t (\tau_a(\boldsymbol{x}, \mathbf{n}, t) + \alpha p(\boldsymbol{x}, t)) \right) \leqslant \beta \tag{17}$$

where α and β are material parameters. In its non-local form, the radius ρ of the integration sphere is an additional parameter for the calculation of Σ_{eq}, defined by Eq. (15). Then, a stress triaxiality ratio can be expressed from the non-local Dang Van criterion quantities:

$$\eta_\gamma = \frac{P_\gamma}{2T_\gamma} \tag{18}$$

where P_γ is the maximum value of the non-local hydrostatic stress and T_γ is the maximum value of the non-local shear stress for a load in the γ direction. For reference loading cases, the value taken by the triaxiality stress ratio are:

- $\eta_\gamma = 0$: full shear stress state
- $\eta_\gamma = 0.33$: uniaxial stress state
- $\eta_\gamma = 0.66$: equibiaxial stress state

Considering an integration sphere radius of 0.4 mm [32], the degree of triaxiality of the reference models of the three welded

structures studied loaded in the e_x direction is: $\eta_{e_x} = 0.50$ for the T joint; $\eta_{e_x} = 0.56$ for the gusset structure; $\eta_{e_x} = 0.47$ for the lap joint. At the weld toes and weld root, the local stress state is multiaxial ($\eta_{e_x} > 0.33$) and the degree of triaxiality is different on the three configurations considered.

For the purpose of comparison, the maximum Dang Van stress $\Sigma_{max,\gamma}$ resulting from the application of a unit load along the γ direction (with $\gamma = e_x, e_y$ or e_z) has been calculated according to:

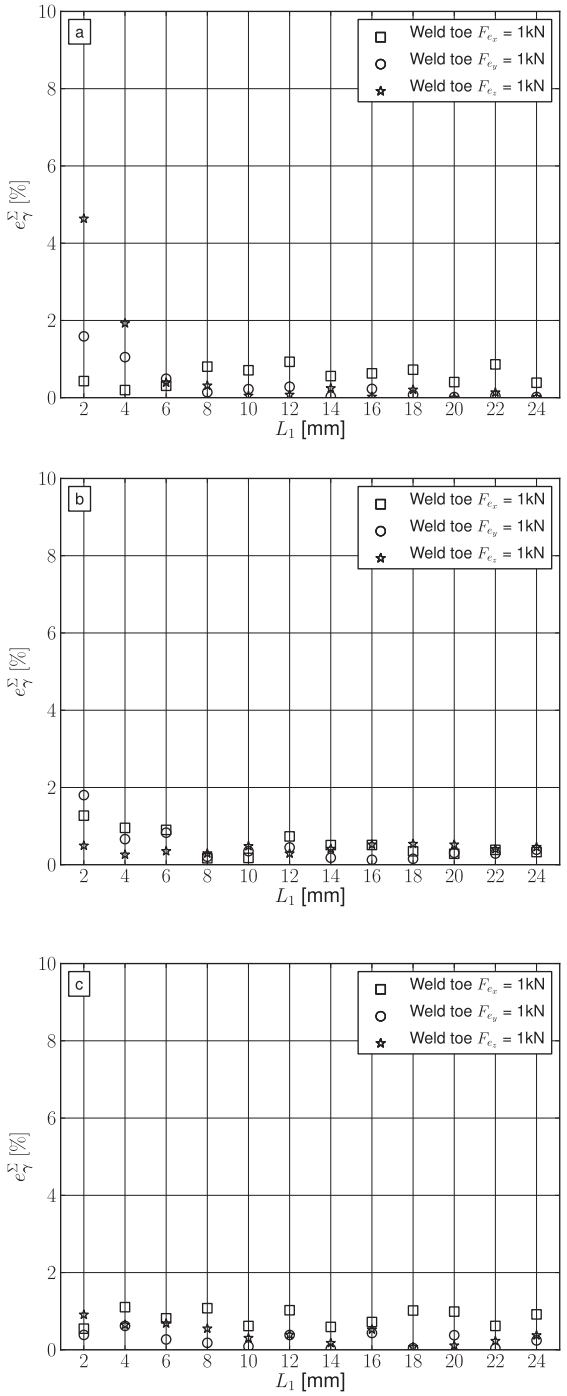

Fig. 9. Evolution of the relative error indicator e_γ^Σ as a function of the L_1 geometrical parameter. Three different welded structures are considered: T-shaped joint (a), gusset (b) and lap joint (c). Three different loading directions are investigated: e_x, e_y and e_z.

$$\Sigma_{max,\gamma} = \max_{x}\left(\Sigma_{eq}(\boldsymbol{x})\right) \tag{19}$$

To evaluate the relative error with respect to the reference solution, the following indicator e_{γ}^{Σ} is used:

$$e_{\gamma}^{\Sigma} = \frac{\left|\Sigma_{max,\gamma}^{r} - \Sigma_{max,\gamma}\right|}{\Sigma_{max,\gamma}^{r}} \tag{20}$$

where $\Sigma_{max,\gamma}^{r}$is the maximum value of the non-local Dang Van criterion obtained from the reference model while $\Sigma_{max,\gamma}$ is the value

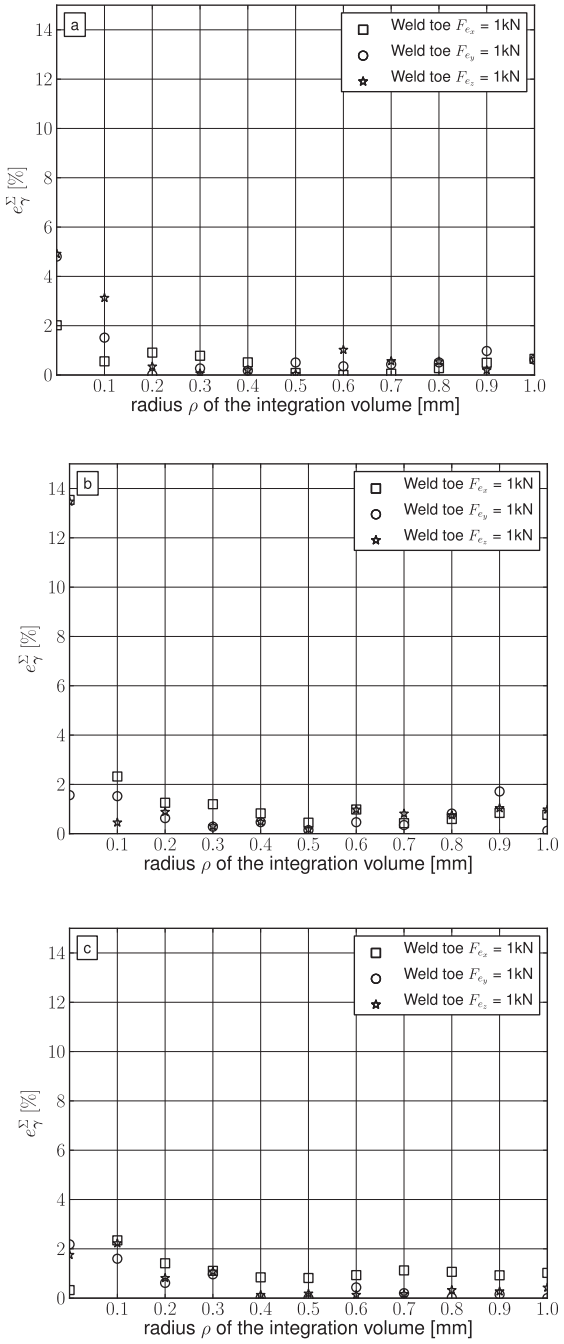

Fig. 10. Evolution of the relative error indicator e_{γ}^{Σ} as a function of the radius of the integration sphere ρ. Three different welded structures are considered: T- shaped joint (a), gusset (b) and lap joint (c), for three different loading directions: $\boldsymbol{e}_x, \boldsymbol{e}_y$ and $\boldsymbol{e}_z$.

calculated from the proposed approach.

3.2.1. Influence of the L_1 and L_2 parameters

To evaluate the impact of the L_1 and L_2 geometrical parameters on the maximum non-local Dang Van stress, the parameters α and ρ must be fixed. Following the suggestion by Fayard et al. [3], a value of 0.33 is used for α. Also, according to Neuber, as cited by Kaffenberger and Vormwald [32], the radius ρ of the integration volume should be set to 0.4 mm.The influence of both parameters α and ρ on the maximum non-local Dang Van stress is discussed in the next sections. The distribution of the relative error e_γ^Σ as a function of L_1 is shown in Fig. 9 for the different welded structures presented in Fig. 7. To calculate the relative error indicator, the L_1 parameter has been varied from 2 to 24 mm. It is seen that for all the structures and loading directions, the maximum errors are observed for the minimum value of L_1. These results are consistent with the fact that, close to the weld toe, the assumption of a plane stress state is incorrect (Section 3.2). It can also be seen that the relative error indicator is inferior to 1% when L_1 exceeds 6 mm, which is the size of the weld throat. When varying the L_2 parameter from 2 to 24 mm, the relative error e_γ^Σ is almost constant and always inferior to 0.1%. It can therefore be concluded that the L_2 parameter has little influence on the accuracy of the proposed method.

3.2.2. Influence of the α parameter

The α parameter, which appears in the definition of the Dang Van criterion, characterizes the sensitivity of a material point to hydrostatic stress. To check whether the proposed approach is valid for any value of this parameter, the relative error has been calculated for the different structures and different loading directions for α ranging from 0 to 0.5. For these calculations, the L_1 parameter has been fixed to 6 mm while the L_2 parameter is fixed equal to 4 mm as before. According to the results, the relative error indicator e_γ^Σ is inferior to 1%, whatever the value of α. This indicates that the proposed approach can be applied to materials with either low or high sensitivity to the hydrostatic stress.

3.2.3. Influence of the ρ parameter

To investigate the influence of ρ, the radius the integration sphere, this parameter has been varied from 0 to 1 mm. The L_1 and L_2 parameters are fixed to 6 mm and 4 mm respectively, while a value of 0.33 is chosen for α. The relative error e_γ^Σ is plotted in Fig. 10 for the different welded structures and loading cases considered here. The error is generally higher for small integration volumes (for $\rho \leqslant 0.1$ mm, $e_\gamma^\Sigma \geqslant 2\%$ for most of the studied cases), for which mesh sensitivity is higher. The proposed approach therefore makes it possible to circumvent the issues associated with mesh sensitivity, as long as the radius ρ of the integration sphere is greater than the element size in the stress concentration zones.

3.3. Conclusion

In this work, an approach based on a two-scale (global–local) model for the fatigue design of large welded structures has been proposed. The objectives are (i) to correctly estimate the stiffness behaviour of welded structures; (ii) to evaluate the local stress field at the weld toes and the weld roots of the different weld configurations found in a chassis structure with limited computational cost; (iii) to apply a non-local multiaxial fatigue criterion to take into account stress gradients and stress multiaxiality in the fatigue design of welded structures.

Local models are first modelled with solid and shell elements. A condensation procedure is applied to obtain the equivalent stiffness matrix associated with each local model. The global model of a welded structure is then built from shell elements while welded connections are replaced by the corresponding equivalent stiffness matrices. After the global computation, a restitution step provides the local stress field in the welded areas, which is used to compute a multiaxial non-local fatigue criterion. The strategy proposed is adapted to large welded structures for a computation time similar to that of a full shell element model.

The influence of the geometrical parameters of the model and the parameters of the fatigue criterion has been studied for three different welded structures for different loading cases. The proposed approach provides accurate estimates of the stiffness of the welded structures without any dependency on geometrical parameters in comparison with full solid element models (less than 0.68%). Also, the Dang Van criterion has been used in a non-local form to evaluate the ability of the proposed method to correctly estimate the stress field. When compared to its applications on full 3D finite element models, the proposed method provide correct estimates of the non-local criterion if (i) the integration volume is large enough ($\rho \geqslant 0.2$mm) and (ii) the solid/shell element interface is far enough from the weld toe (6 mm).

Future work will consist of carrying out fatigue tests on different welded structures to identify the fatigue criterion parameters and to validate the fatigue prediction of the proposed model.

Declaration of Competing Interest

The authors declare that they have no known competing financial interests or personal relationships that could have appeared to influence the work reported in this paper.

Acknowledgements

This research is supported by the Manitou company and the National Association of Research and Technology (ANRT).

References

[1] A. Hobbacher, Recommendations for Fatigue Design of Welded Joints and Components, second ed., International institute of welding, 2016.
[2] D. Radaj, C. Sonsino, W. Fricke, Fatigue Assessment of Welded Joints by Local Approaches, second ed., Woodhead Publishing, 2006.
[3] J. Fayard, A. Bignonnet, K. Dang Van, Fatigue design criterion for welded structures, Fatigue Fract. Eng. Mater. Struct. 19 (1996) 723–729, https://doi.org/10.1111/j.1460-2695.1996.tb01317.x.
[4] K. Dang Van, Sur la résistance à la fatigue des métaux, Ph.D. thesis, 1973.
[5] D. Radenkovic, Analyse des contraintes dans les joints tubulaires, Institut de recherches de la sidérerurgie française, 1981.
[6] M. Fermér, H. Svensson, Industrial experiences of fe-based fatigue life predictions of welded automotive structures, Fatigue Fract. Eng. Mater. Struct. 24 (2001) 489–500, https://doi.org/10.1046/j.1460-2695.2001.00409.x.
[7] D. Turlier, P. Klein, F. Bérard, Fea shell element model for enhanced structural stress analysis of seam welds, Weld. World 58 (2014) 511–528, https://doi.org/10.1007/s40194-014-0134-y.
[8] P. Dong, A structural stress definition and numerical implementation for fatigue analysis of welded joints, Int. J. Fatigue 23 (2001) 865–876, https://doi.org/10.1016/S0142-1123(01)00055-X.
[9] W. Fricke, A. Kahl, H. Paetzold, Fatigue assessment of root cracking of fillet welds subject to throat bending using the structural stress approach, Weld. World 50 (2006) 64–74, https://doi.org/10.1007/BF03266538.
[10] T. Boukharouba, T. Tamine, L. Niu, C. Chehimi, G. Pluvinage, The use of notch stress intensity factor as a fatigue crack initiation parameter, Eng. Fract. Mech. 52 (1995) 503–512, https://doi.org/10.1016/0013-7944(94)00242-A.
[11] G. Meneghetti, B. Atzori, G. Manara, The peak stress method applied to fatigue assessments of steel tubular welded joints subject to mode-i loading, Eng. Fract. Mech. 77 (2010) (2009) 2100–2114, https://doi.org/10.1016/j.engfracmech.2010.04.002, international Conference on Crack Paths.
[12] U. Zerbst, M. Madia, B. Schork, J. Hensel, P. Kucharczyk, D. Ngoula, D. Tchuindjang, J. Bernhard, C. Beckmann, Fatigue and Fracture of Weldments: The IBESS Approach for the Determination of the Fatigue Life and Strength of Weldments by Fracture Mechanics Analysis, Springer, 2019, https://doi.org/10.1007/978-3-030-04073-4.
[13] P. Lazzarin, R. Zambardi, A finite volume energy based approach to predict the static and fatigue behavior of components with sharp v-shaped notches, Int. J. Fract. 112 (2001) 275–298.
[14] D. Turlier, M. Facchinetti, S. Wolf, I. Raoult, B. Delattre, A. Magnin, N. Grimonprez, Seam weld shell element model for thin walled structure fe fatigue design, MATEC Web Conf. 165 (2018) 21007, https://doi.org/10.1051/matecconf/201816521007.
[15] J. Fayard, Dimensionnement a la fatigue polycyclique de structures soudees, Ph.D. thesis, Sciences appliquées. Physique Palaiseau, Ecole polytechnique 1996, 1996. http://www.theses.fr/1996EPXXA040, thèse de doctorat dirigée par Dang Van, Ky.
[16] D. Radaj, C. Sonsino, Fatigue Assessment of Welded Joints by Local Approaches, second ed., Abington Publishing, 1998.
[17] N. Zettlemoyer, J. Fisher, Stress Gradient Correction Factor for Stress Intensity at Welded Stiffeners and Cover Plates, Technical Report, 1977.
[18] F. Dal Cero Coehlo, Fatigue Life Assessment of Welded Joints, Theses, ISAE-ENSMA Ecole Nationale Supérieure de Mécanique et d'Aérotechique – Poitiers, 2014. https://tel.archives-ouvertes.fr/tel-01127338.
[19] K. Shim, D. Monaghan, C. Armstrong, Mixed dimensional coupling in finite element stress analysis, Eng. Comput. 18 (2002) 241–252, https://doi.org/10.1007/s003660200021.
[20] R. McCune, C. Armstrong, D. Robinson, Mixed-dimensional coupling in finite element models, Int. J. Numer. Meth. Eng. 49 (2000) 725–750, https://doi.org/10.1002/1097-0207(20001030)49:6<725::AID-NME967>3.0.CO;2-W.
[21] A. L'Houcine, Développement d'éléments finis de coque pour le calcul des ouvrages d'art, Theses, Ecole Nationale des Ponts et Chaussées, 1984. https://pastel.archives-ouvertes.fr/tel-00529363.
[22] D. Taylor, CHAPTER 2 – The Theory of Critical Distances: Basics: An Introduction to the Basic Methodology of the TCD, Elsevier Science Ltd, Oxford, 2007. doi: https://doi.org/10.1016/B978-008044478-9/50003-X.
[23] D. Taylor, Geometrical effects in fatigue: a unifying theoretical model, Int. J. Fatigue 21 (1999) 413–420, https://doi.org/10.1016/S0142-1123(99)00007-9.
[24] D. Taylor, A mechanistic approach to critical-distance methods in notch fatigue, Fatigue Fract. Eng. Mater. Struct. 24 (2001) 215–224, https://doi.org/10.1046/j.1460-2695.2001.00401.x, cited By 94.
[25] P. Livieri, R. Tovo, Overview of the geometrical influence on the fatigue strength of steel butt welds by a nonlocal approach, Fatigue Fract. Eng. Mater. Struct. 43 (2020) 502–514, https://doi.org/10.1111/ffe.13135.
[26] F. Morel, T. Palin-Luc, A non-local theory applied to high-cycle multiaxial fatigue, Fatigue Fract. Eng. Mater. Struct. 25 (2002) 649–665, https://doi.org/10.1046/j.1460-2695.2002.00527.x.
[27] L. Susmel, D. Taylor, A critical distance/plane method to estimate finite life of notched components under variable amplitude uniaxial/multiaxial fatigue loading, Int. J. Fatigue 38 (2012) 7–24, https://doi.org/10.1016/j.ijfatigue.2011.11.015.
[28] J. Batoz, G. Dhatt, Modélisation des structures par éléments finis: Coques, Modélisation des structures par éléments finis, Hermes Science Publications, 1992. https://books.google.fr/books?id=zwt_AAAACAAJ.
[29] C. Geuzaine, J. Remacle, Gmsh: A 3-d finite element mesh generator with built-in pre- and post-processing facilities, Int. J. Numer. Meth. Eng. 79 (2009) 1309–1331, https://doi.org/10.1002/nme.2579, arXiv:https://onlinelibrary.wiley.com/doi/pdf/10.1002/nme.2579.
[30] P.R. Amestoy, I.S. Duff, J. Koster, J. L'Excellent, A fully asynchronous multifrontal solver using distributed dynamic scheduling, SIAM J. Matrix Anal. Appl. 23 (2001) 15–41, https://doi.org/10.1137/S0895479899358194.
[31] A. Callens, A. Bignonnet, Fatigue design of welded bicycle frames using a multiaxial criterion, Procedia Eng. 34 (2012) 640–645, https://doi.org/10.1016/j.proeng.2012.04.109, eNGINEERING OF SPORT CONFERENCE 2012.
[32] M. Kaffenberger, M. Vormwald, Considering size effects in the notch stress concept for fatigue assessment of welded joints, Comput. Mater. Sci. 64 (2012) 71–78, https://doi.org/10.1016/j.commatsci.2012.02.047.